LPSC XLIX #2362

Searching for Buried Water Ice in Martian Dunes with Radar and Thermal Data

Nathaniel Putzig [1] & Rachael Hoover.[2] [1] Planetary Science Institute, Lakewood, Colorado, USA. nathaniel@putzig.com. [2] Southwest Research Institute, Boulder, Colorado, USA.

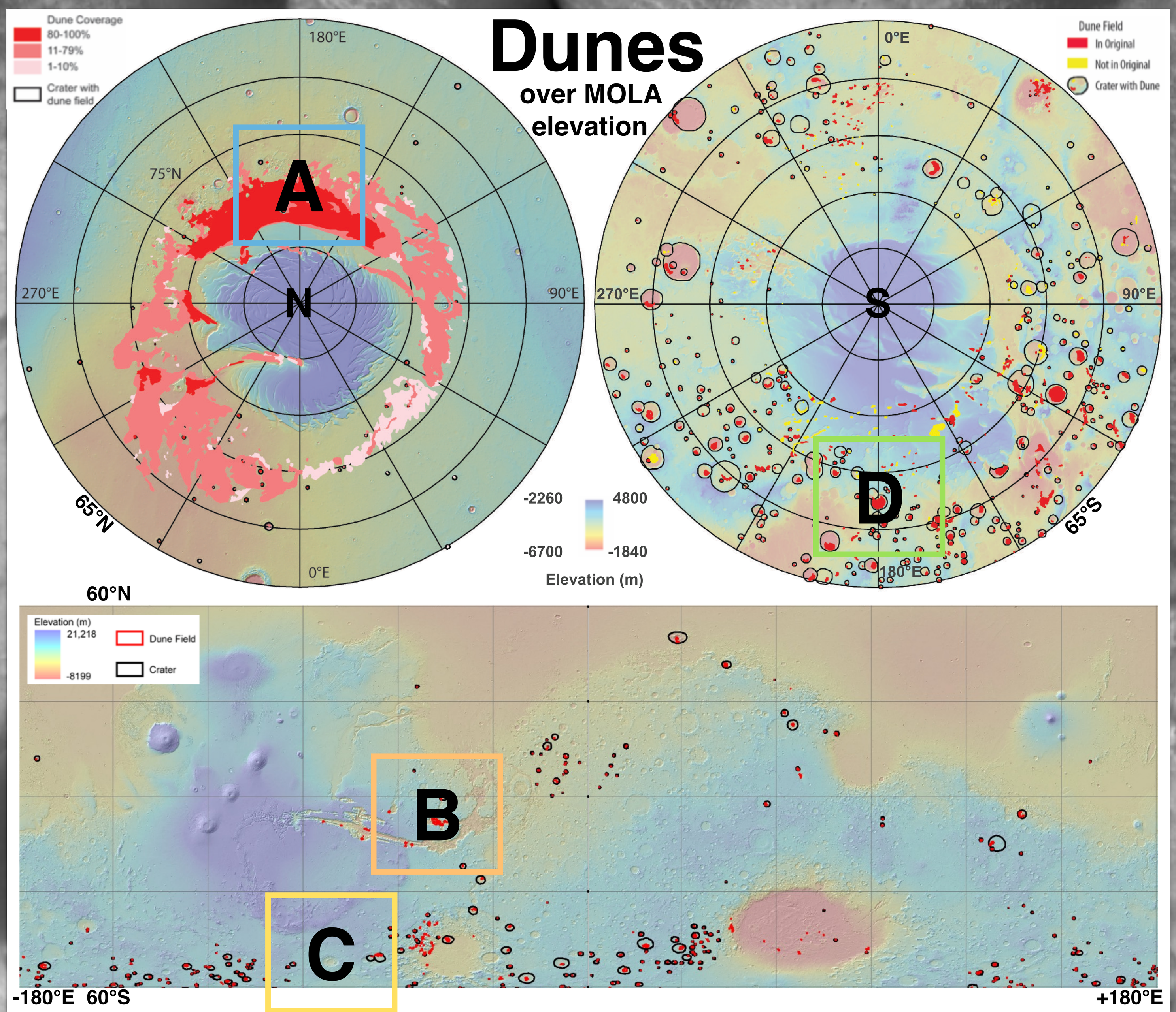

Dune maps by Hayward et al. (2007, 2010, 2012) [1-3]

The Mars Reconnaissance Orbiter Shallow Radar transmits pulses at 15–25 MHz from a ~300-km orbit, yielding wavelengths of 15 m in free space, ~8.5 m in water ice, and ~5.5 m in basaltic materials and a lateral resolution of ~3–6 km, reducible along-track to 0.3–1 km with SAR processing [4]. Returns from the nadir surface may be followed by others from subsurface geologic boundaries and off-nadir surface topography. Roughness, such as dune forms at radar-wavelength scales, can induce scattering and reduce the power and coherence of returns.

Brightness temperatures calculated from Mars Global Surveyor Thermal Emission Spectrometer observations are used to derive thermal inertia, the primary driver of Martian diurnal temperature oscillations [5]. Results have been mapped globally at 3 km resolution and seasonally at 10° Ls [6]. Rocks, ice, duricrust, sand, and dust all contribute differently to observed temperatures, and the derived thermal inertia at any given location may vary with time of day and season in a way that depends on mixtures or layering of these different materials. Thus, thermal modeling of heterogeneous materials may be used to constrain surface material variations.

Conclusions

The lateral resolution of SHARAD limits its utility in dune studies to larger fields. SHARAD's wavelength is similar to the scale of many dune forms, further limiting its use to those fields with relatively muted surface features. Such fields of smaller dunes or sand sheets typically allow radar signals to penetrate and reflect from interior or underlying interfaces. These cases yield information about layering within and beneath dunes, providing data relevant to dune formation and evolution and associated climate history.

TES also has relatively coarse lateral resolution, and the coverage is not complete for all seasons at any given location. Variations of apparent thermal inertia as derived from TES data are indicative of heterogeneity, but the results can sometimes be equivocal or at odds with inferences made from images and morphological data [9].

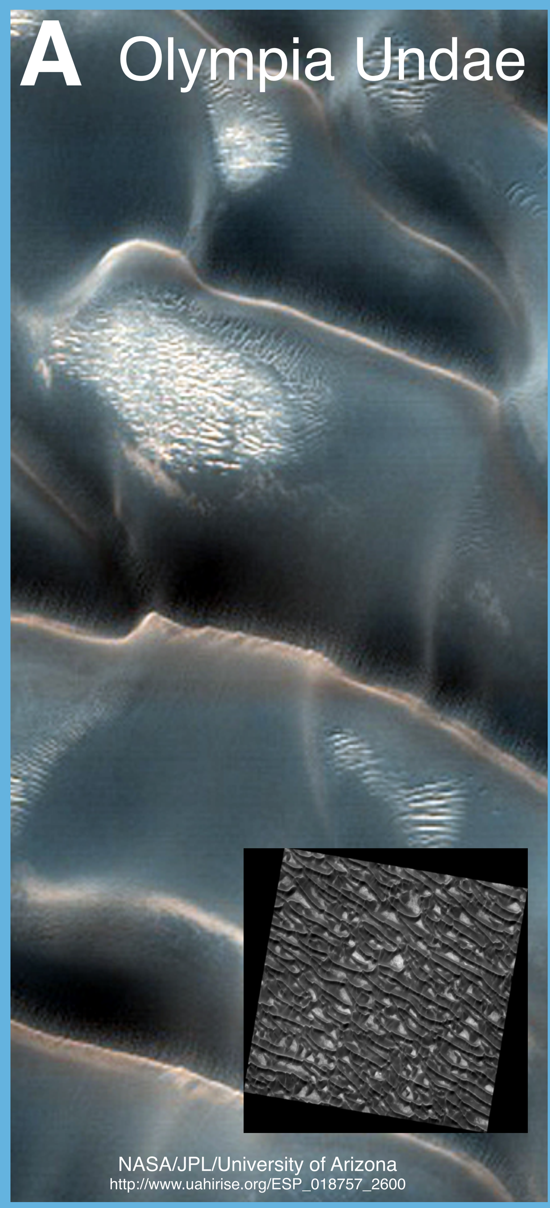

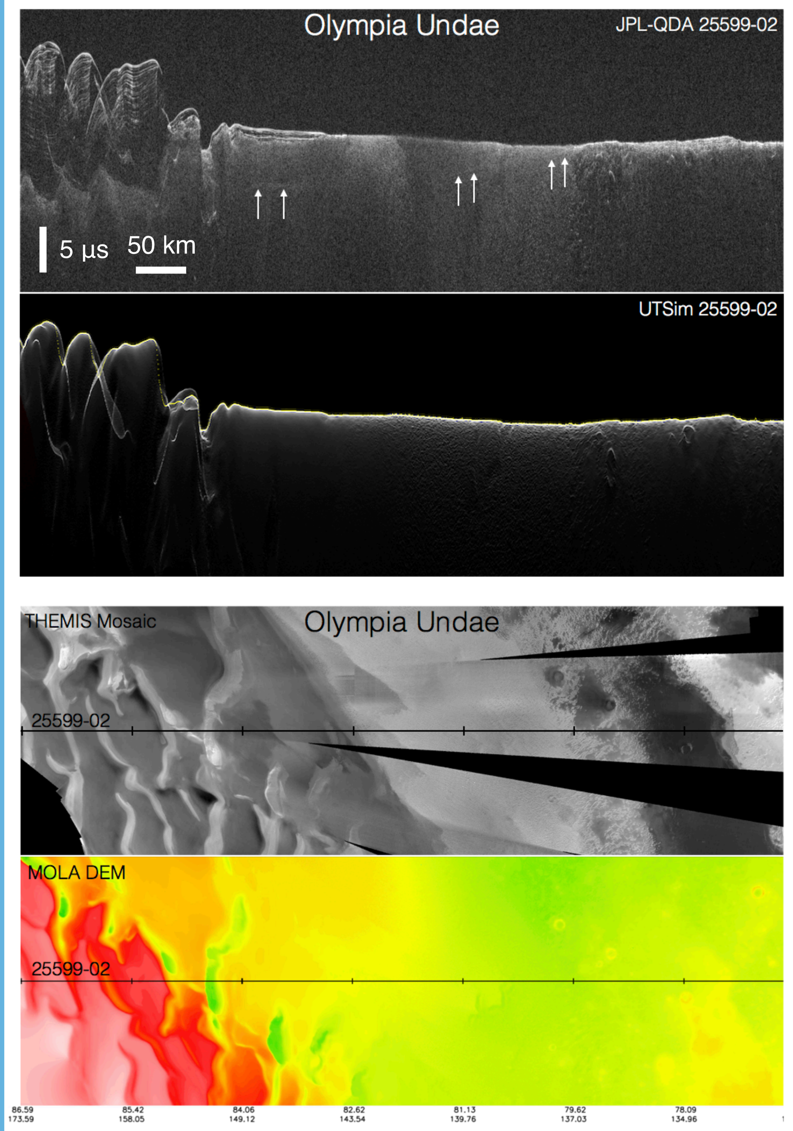

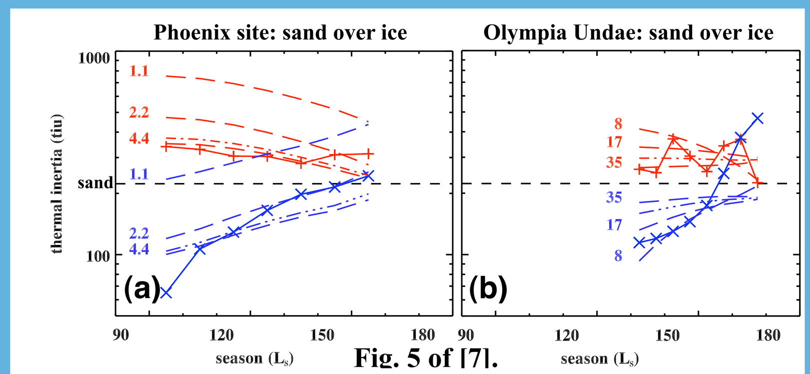

Fig. 5 of [7].

Seasonal variations in apparent thermal inertia from TES (+, × symbols) and layered models (dashed lines) at 2AM (blue) and 2PM (red) local times. Best-fitting models (dash-dotted lines) indicate (a) 4.4 cm of sand over ice at the Phoenix site (matches the lander-observed depth to ice) and (b) 27 cm of sand over ice in Olympia Undae (accounts for thermal behavior of dunes).

SHARAD observations of Olympia Undae have diffuse surface returns, rarely show faint subsurface returns (at arrows) that likely represent the Vastitas Borealis deposits below the sand. Simulations have no features corresponding to the deep returns nor to layering in the polar deposits & Olympia Planum.

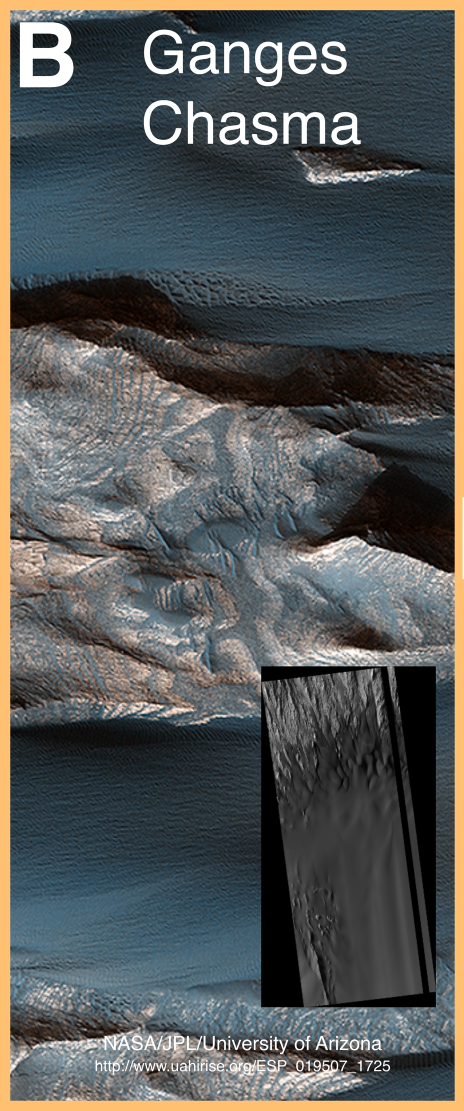

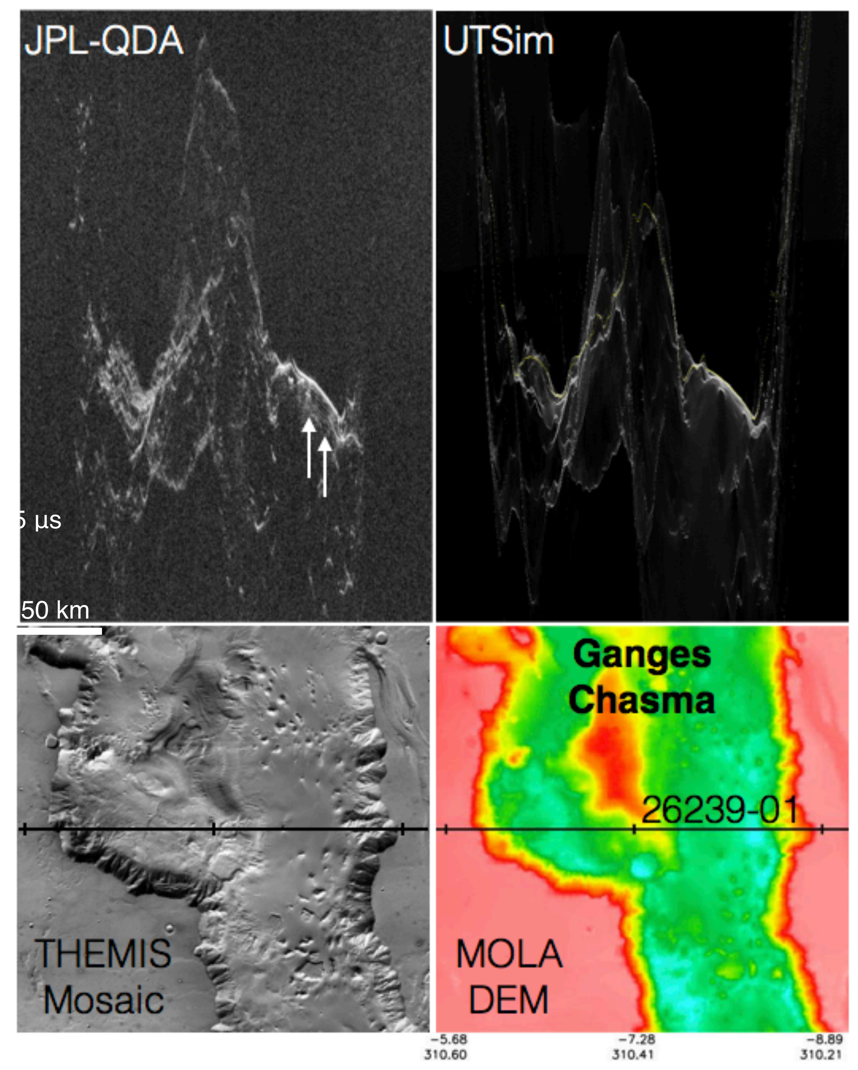

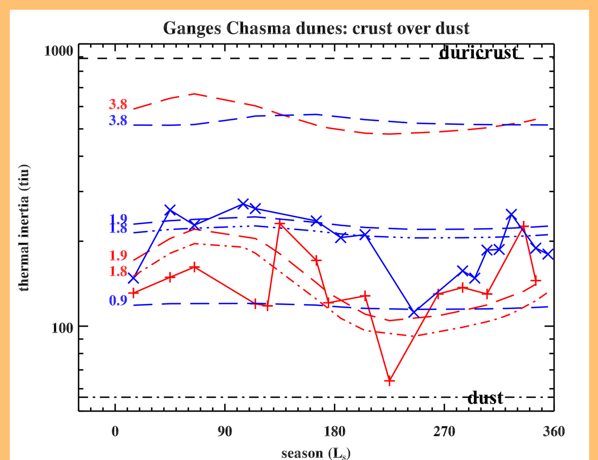

Seasonal variations in apparent thermal inertia from TES (+, × symbols) and layered models (dashed lines) at 2AM (blue) and 2PM (red) local times. Best-fitting model (dash-dotted lines) indicate 1.8 cm of duricrust over dust for Ganges Chasma dunes. Misfit may indicate more complexity.

Features on the surface of sand dunes in Ganges Chasma are of a scale below the SHARAD wavelength, and they produce strong surface returns. Fainter returns often follow, with a slightly stronger, more coherent return (arrows) at a delay of ~2 µs (122 m for sand dielectric of 6) that may represent the base of the sand. Lack of corresponding returns in the clutter simulation supports the interpretation that the late returns are from subsurface interfaces.

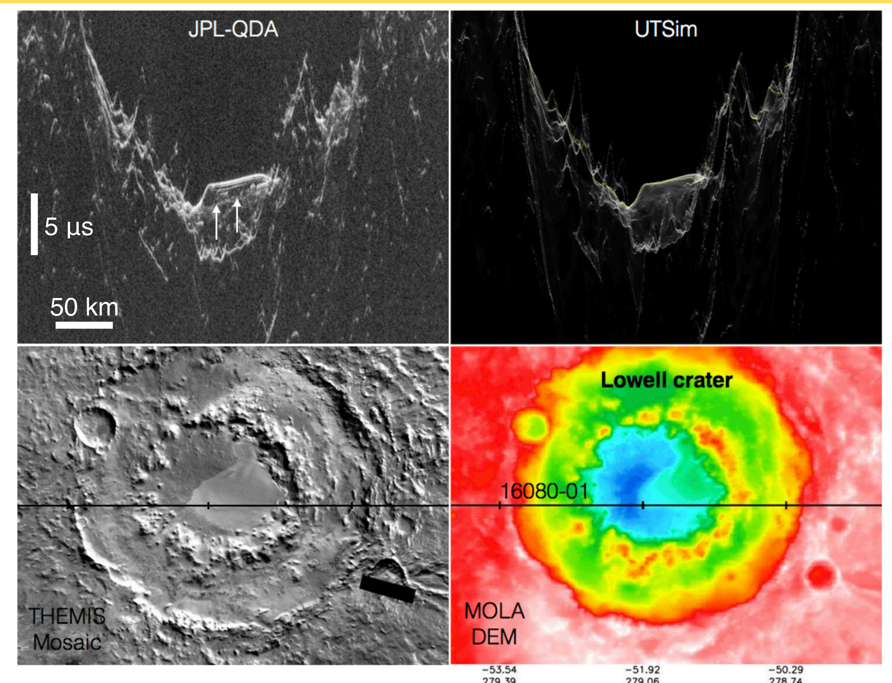

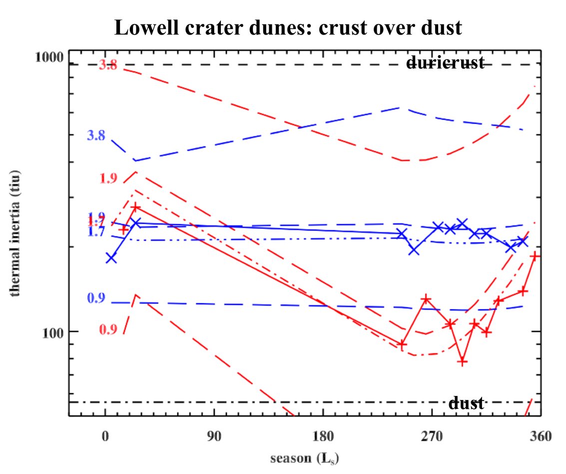

Seasonal variations in apparent thermal inertia from TES (+, × symbols) and layered models (dashed lines) at 2AM (blue) and 2PM (red) local times. Best-fitting model (dash-dotted lines) indicate 1.7 cm of duricrust over dust for Lowell crater dunes.

The dune field at the center of Lowell crater yields a strong surface return followed by a weaker return (at arrows on radargram) at a delay of ~1.4 µs (86 m for a sand dielectric of 6) that may be from either the crater floor or another boundary such as ground ice. The strong surface return is consistent with dune forms (or a sand sheet) well below the ~15-m scale of SHARAD. Lack of a corresponding return in the clutter simulation supports a subsurface source for the late return.

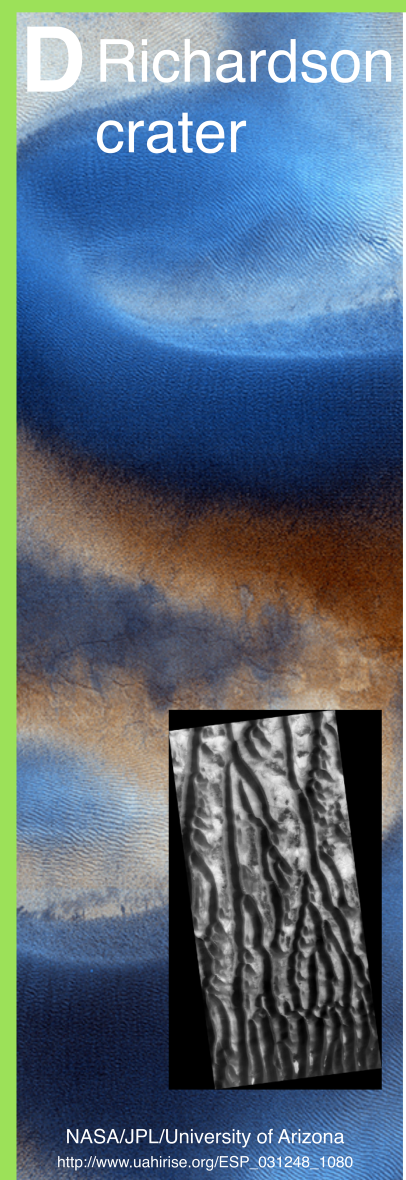

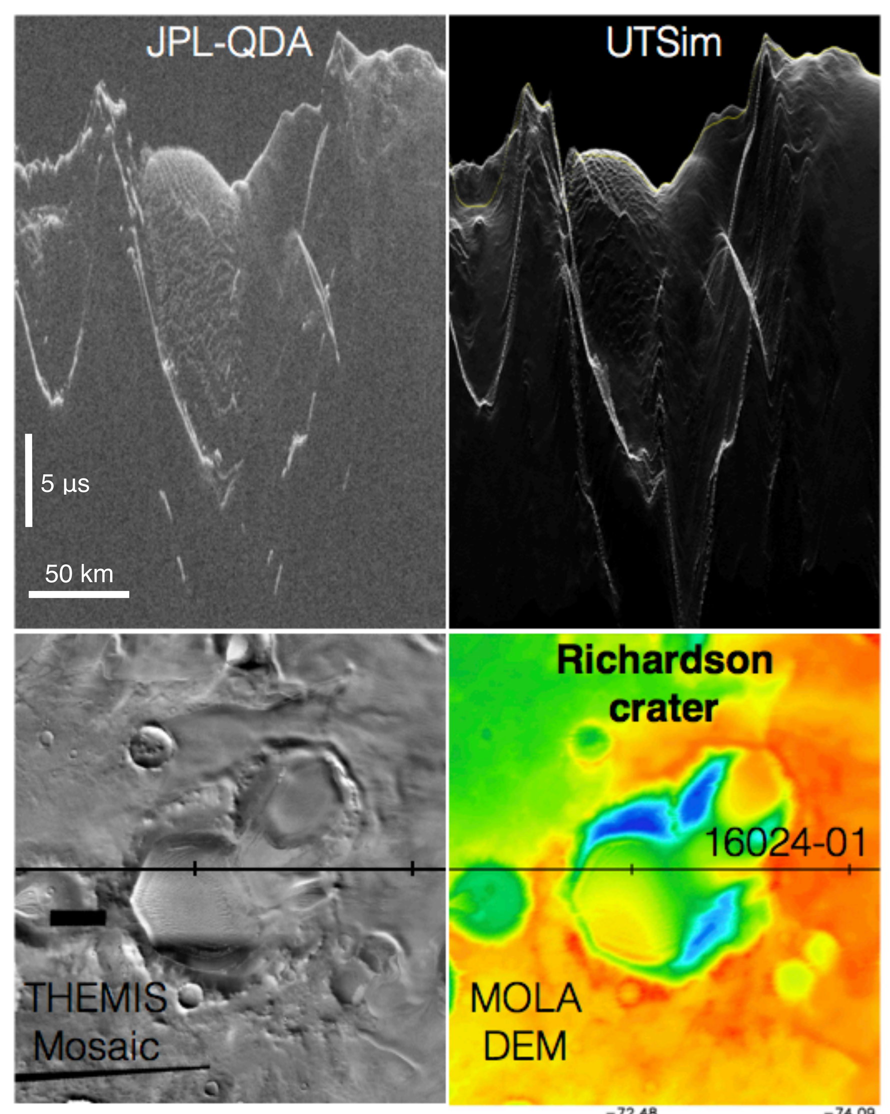

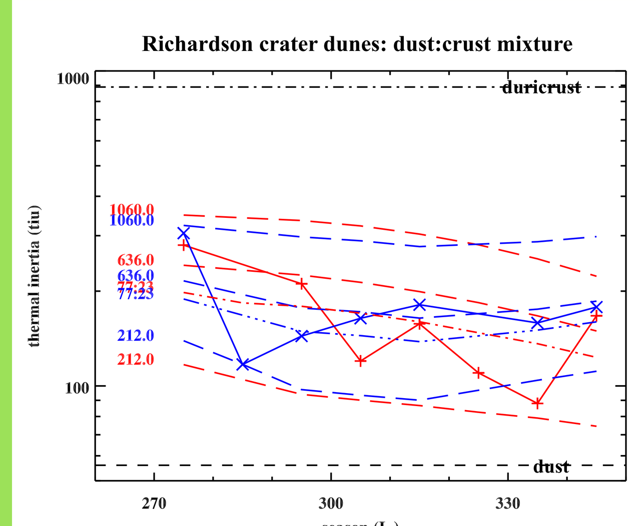

Seasonal variations in apparent thermal inertia from TES (+, × symbols) and layered models (dashed lines) at 2AM (blue) and 2PM (red) local times. Best-fitting model (dash-dotted lines) indicate a lateral mixture of 77% dust and 23% duricrust for Richardson crater dunes. However, the fit is not ideal and other factors may be involved in the observed thermal behavior.

Richardson crater (on the periphery of the south polar layered deposits, SPLD) contains mounds that are likely composed largely of water ice. Extensive dunes on the scale of the SHARAD wavelength occur at the surface and result in diffuse radar returns. Simulations show nearly all the features seen in the radargrams, indicating surface sources and no evidence for subsurface returns. Unlike in the north, many areas of the SPLD are subject to diffuse returns that may be precluding the detection of deeper layering [8].

References

[1] Hayward R. K. et al. (2007) USGS Open File Report 2007-1158. [2] Hayward R. K. et al. (2010) USGS Open File Report 2010-1170. [3] Hayward R. K. et al. (2012) USGS Open File Report 2012-1259. [4] Seu R. et al. (1997) JGR 112, E05S05. [5] Mellon et al. (2008) Ch. 18 in Bell III, J. F., ed., 2008, Cam. U. Press. ISBN: 9780521866989. [6] Putzig and Mellon (2007) Icarus 191, 68-94. [7] Putzig et al. (2014) Icarus 230, 64-76. [8] Campbell et al. (2015) Lunar Planet. Sci. XLVI, Abstract 2366. [9] Hoover et al. (2018) Lunar Planet. Sci. XLIX, Abstract 1811. [10] Plaut J. J. et al. (2009) GRL 36, L02203. [11] Choudhary P. et al. (2016) IEEE Geosci. Remote Sensing Lett. 13, 1285-1289. [12] Edwards C. S. et al. (2011) JGR 116, E10008. [13] Smith et al. (2003) NASA PDS MGS-M-MOLA-5-MEGDR-L3-V1.0.

Acknowledgements

SHARAD was provided to NASA's MRO by the Italian Space Agency (ASI). Its operations are led by the DIET Department, University of Rome "La Sapienza" under an ASI contract. Radargrams and simulations were produced in the Colorado Shallow Radar Processing System (CO-SHARPS) with codes developed by the Jet Propulsion Laboratory (i.e., that used by [10]) and the University of Texas [11]. THEMIS mosaics are from [12] and MOLA DEMs are created in CO-SHARPS from PDS data [13]. We are grateful for support of these efforts from the MRO Project and the SHARAD Team. TES results use thermal analysis tools available at http://marstherm.psi.edu/. This work is partially supported by NASA grant NNX17AB25G.